Inorganic Chemistry
Cite This: Inorg. Chem. 2018, 57, 11864−11873
Article
pubs.acs.org/IC

In Situ ^{27}Al NMR Spectroscopy of Aluminate in Sodium Hydroxide Solutions above and below Saturation with Respect to Gibbsite

Trent R. Graham,[†,#] Mateusz Dembowski,[‡,#] Ernesto Martinez-Baez,[§] Xin Zhang,[‡] Nicholas R. Jaegers,[†,‡] Jianzhi Hu,[‡] Miroslaw S. Gruszkiewicz,[∥] Hsiu-Wen Wang,[∥] Andrew G. Stack,[∥] Mark E. Bowden,[‡] Calvin H. Delegard,[⊥] Gregory K. Schenter,[‡] Aurora E. Clark,[§] Sue B. Clark,[‡,§] Andrew R. Felmy,[‡,§] Kevin M. Rosso,[‡] and Carolyn I. Pearce*[,‡]

[†]The Voiland School of Chemical and Biological Engineering, Washington State University, Pullman, Washington 99164, United States
[‡]Pacific Northwest National Laboratory, Richland, Washington 99352, United States
[§]Department of Chemistry, Washington State University, Pullman, Washington 99164, United States
[∥]Oak Ridge National Laboratory, Oak Ridge, Tennessee 37831, United States
[⊥]TradeWind Services LLC, Richland, Washington 99352, United States

Supporting Information

ABSTRACT: Aluminum hydroxide ($Al(OH)_3$, gibbsite) dissolution and precipitation processes in alkaline environments play a commanding role in aluminum refining and nuclear waste processing, yet mechanistic aspects underlying sluggish kinetics during crystallization have remained obscured due to a lack of in situ probes capable of isolating incipient ion pairs. At a molecular level Al is cycling between tetrahedral (T_d) coordination in solution to octahedral (O_h) in the solid. We explored dissolution of $Al(OH)_3$ that was used to produce variably saturated aluminate ($Al(OH)_4^-$)-containing solutions under alkaline conditions (pH >13) with in situ ^{27}Al magic angle spinning (MAS)−nuclear magnetic resonance (NMR) spectroscopy, and interrogated the results with ab initio molecular dynamics (AIMD) simulations complemented with chemical shift calculations. The collective results highlight the overall stability of the solvation structure for T_d Al in the $Al(OH)_4^-$ oxyanion as a function of both temperature and Al concentration. The observed chemical shift did not change significantly even when the Al concentration in solution became supersaturated upon cooling and limited precipitation of the octahedral $Al(OH)_3$ phase occurred. However, subtle changes in $Al(OH)_4^-$ speciation correlated with the dissolution/precipitation reaction were found. AIMD-informed chemical shift calculations indicate that measurable perturbations should begin when the $Al(OH)_4^-\cdots Na^+$ distance is less than 6 Å, increasing dramatically at shorter distances, coinciding with appreciable changes to the electrostatic interaction and reorganization of the $Al(OH)_4^-$ solvation shell. The integrated findings thus suggest that, under conditions incipient to and concurrent with gibbsite crystallization, nominally expected contact ion pairs are insignificant and instead medium-range (4−6 Å) solvent-separated $Al(OH)_4^-\cdots Na^+$ pairs predominate. Moreover, the fact that these medium-range interactions bear directly on resulting gibbsite characteristics was demonstrated by detailed microscopic and X-ray diffraction analysis and by progressive changes in the fwhm of the O_h resonance, as measured by in situ NMR. Sluggish gibbsite crystallization may arise from the activation energy associated with disrupting this robust medium-range ion pair interaction.

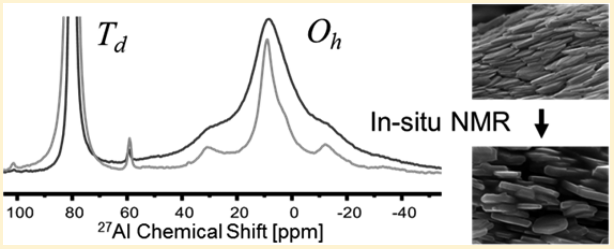

1. INTRODUCTION

Understanding the precipitation and dissolution behavior of the thermodynamically stable aluminum hydroxide phase gibbsite ($Al(OH)_3$) in high-pH environments from a kinetic and mechanistic standpoint has been a matter of concern for well over a century. Thus, gibbsite precipitation is central to the Bayer process, but its dissolution/reprecipitation behavior also is key to important ongoing cases of nuclear waste processing.[1,2] The initial stages of the Bayer process involve dissolution of aluminum from bauxite ores containing aluminum hydroxides and oxyhydroxides using heat and concentrated sodium hydroxide. Dissolution is followed by decantation and then cooling and dilution of the pregnant liquors with water, thus making them highly supersaturated with respect to gibbsite precipitation. Generous gibbsite seeding accelerates crystallization of purified gibbsite from these supersaturated solutions.[3] For processing of high-level nuclear waste consisting of caustic, near- and supersaturated aluminate liquors, uncontrolled gibbsite precipitation upon

Received: March 8, 2018
Published: July 23, 2018

DOI: 10.1021/acs.inorgchem.8b00617
Inorg. Chem. 2018, 57, 11864−11873

cooling and dilution can lead to (i) accumulation of settled solids occupying usable tank space, (ii) fouling during ion exchange operations, and (iii) plugging of transfer lines.[2] Studies of the effect of processing parameters (sodium hydroxide concentration, temperature, etc.) are usually performed by analyzing samples heated in autoclaves at various time intervals.[1,4,5] The results are analyzed to develop thermodynamic Pitzer models[6] and kinetic models,[7] but the predictive power of these models is not sufficiently comprehensive: for example, in the presence of other salts.[2] Thus, developing a predictive understanding of supersaturated aluminate ($Al(OH)_4^-$) solutions in NaOH, to control dissolution/precipitation reactions, would have significant environmental benefits through both improvements in energy efficiency during aluminum production and acceleration of nuclear waste processing.

The essence of gibbsite precipitation and dissolution reactions entails aluminum coordination changes from tetrahedral (four-coordinate, T_d) dissolved species to octahedral (six-coordinate, O_h) solid phases, and vice versa. For dissolution under acidic or neutral conditions, rates are intrinsically linked to solution-phase species;[8,9] therefore, it is likely that speciation is key in alkaline environments as well.[10] The dominant species present in caustic Al mixtures is widely accepted to be the tetrahedrally coordinated aluminate ion, $Al(OH)_4^-$.[11,12] The formation of tetrahedrally coordinated dimeric species, such as $Al_2O(OH)_6^{2-}$ at [Al] > 1.0 M, has also been proposed on the basis of Raman, nuclear magnetic resonance (NMR), and conductivity measurements.[12−17] The structure of the dimer in terms of whether it is oxy-bridged versus hydroxy-bridged or instead existing as an unbridged ion−ion aggregate is still under debate.[11,18,19] Both the monomeric and polymeric Al species are proposed to be stabilized with labile alkali ions.[20] At high concentrations, closely packed $Na^+Al(OH)_4^-$ ion pairs and solvent molecules are consistent with dielectric relaxometry studies in 8 M NaOH, but measurements were not sensitive to the other species.[21] The viscosity of supersaturated caustic $Al(OH)_4^-$ solutions is strongly influenced by these ion−ion and ion−solvent interactions. Thus, the species in caustic solutions above and below saturation with respect to gibbsite are still a matter of debate, despite their importance to understanding mechanisms of precipitation and dissolution.[22]

There is a complex relationship among the concentrations of Al, OH^- and Na^+ in the system. Once beyond concentrations of 5 M NaOH and 3 M Al, the system changes from gibbsite controlled solubility to sodium aluminate controlled solubility. In this regime, increasing the NaOH concentration at constant [Al] leads to the formation of $Na^+Al(OH)_4^-$ contact ion pairs and dimeric species, which act to stabilize higher [Al] in solution and lead to spectroscopic signatures such as an upfield shift in the ^{27}Al NMR signal.[23] However, increasing the [Al] relative to [NaOH] drives the system toward gibbsite precipitation, but in this regime, i.e. <3 M and [NaOH] <5 M, solution-phase changes are more challenging to probe spectroscopically.

In the present study, we combine in situ ^{27}Al magic angle spinning (MAS) nuclear magnetic resonance (NMR) spectroscopy with ab initio molecular dynamics (AIMD) simulations to closely examine speciation, solvation, and ion−ion effects in caustic sodium aluminate solutions under conditions entailing (i) supersaturation in the absence of a solid phase, (ii) saturation with coexisting gibbsite, and (iii) solutions below the solubility limit with respect to gibbsite, to further our understanding of the nucleation and precipitation of $Al(OH)_3$ nanoparticles. Experimental conditions were selected on the basis of gibbsite solubility in the 3 M NaOH system, calculated using an updated Pitzer virial-coefficient approach. This NaOH concentration was selected to represent concentrations of relevance to high-level nuclear waste stored in large quantities at the Hanford Site, Washington, USA. In situ MAS NMR that is capable of operating under elevated temperature and pressure conditions[24] was used to monitor the dissolution of gibbsite as a function of temperature. The solubility of gibbsite in strongly alkaline solution increases steeply with temperature. These variable-temperature experiments, conducted up to 100 °C to attain hydrothermal conditions, enabled the preparation and analysis of supersaturated $Al(OH)_4^-$ solutions containing more dissolved Al than is predicted to be thermodynamically stable at lower temperatures for a 3 M NaOH solution. Conditions (temperature, time, and [NaOH]) were selected to maximize the [Al] in solution, but without the solid phase transitioning to boehmite.[25] The NMR experiments, probing both the solid and solution Al species simultaneously, were combined with (i) ex situ ^{27}Al NMR to probe the solution phase and (ii) X-ray diffraction (XRD) and scanning electron microscopy (SEM) to characterize the solid phase.

Direct comparison of NMR chemical shifts with high-level computational simulations is a distinguishing feature of this study. In previous work computations have consisted of quantum mechanical gas phase and first-shell solvated Al species cluster calculations (with and without inclusion of continuum solvation effects), wherein the presence of the aforementioned Al dimers has been mostly supported and other possible intermediary species in the gibbsite formation process have been proposed.[26] However, it has been recognized[26] that inclusion of an explicit solvation environment beyond the first solvation shell is needed to describe $Al(OH)_4^-$ thermal geometric fluctuations as well as its interaction with counterions (e.g., Na^+). Although classical MD has been employed to examine $Na^+Al(OH)_4^-$ ion pair formation,[27] AIMD provides a unique opportunity to study the influence of cation interactions with $Al(OH)_4^-$ on spectroscopic features: e.g., ^{27}Al NMR. NMR shielding tensor calculations have been previously used to probe speciation as well as molecular environment fluctuations around metallic centers such as Pt.[28] Correlating calculated NMR spectroscopic observables with specific molecular configurational changes around or near the NMR-active nuclei can be accurately achieved, as is done here, by (i) performing first-principles molecular dynamic simulations with explicit inclusion of the solvation environment, (ii) statistical sampling of the generated configurational ensemble, and (iii) consequent quantum mechanical cluster NMR shielding tensor calculations followed by (iv) structural analysis to explore different possible contributions to the calculated observable.[28−30]

Thus, we have examined correlations between ^{27}Al NMR isotropic chemical shielding and specific aluminate molecular configurational changes via density functional theory (DFT) gauge-including atomic orbitals (GIAO) NMR cluster calculations statistically sampled from AIMD trajectories (referred to hereafter as AIMD/DFT).

These novel in situ NMR variable-temperature experiments, complemented with chemical shift calculations based on high-

DOI: 10.1021/acs.inorgchem.8b00617
Inorg. Chem. 2018, 57, 11864−11873

level theory, highlight the overall stability of the solvation structure for T_d Al in the $Al(OH)_4^-$ anion, with the chemical shift varying very little as a function of both temperature and Al concentration. The chemical shift, and thus the solvation structure, did not change significantly even when the Al concentration in solution became supersaturated upon cooling from 80 or 100 °C to room temperature: i.e., [Al] of up to 1.0 M existed at room temperature, despite a thermodynamically derived solubility limit of 0.245 M, and no observable precipitation of an octahedral $Al(OH)_3$ phase was observed in the 1 M system over several hours. However, subtle changes in $Al(OH)_4^-$ solution speciation were detected and are correlated with perturbations of the dissolution/precipitation reaction. At the same time, the AIMD/DFT-predicted change to the ^{27}Al NMR as a function of the $Al(OH)_4^-\cdots Na^+$ distance indicates that the chemical shift begins to be perturbed below 6 Å. This change increases dramatically as the distance is decreased and coincides with appreciable changes in electrostatic interactions between the ions and reorganization of the $Al(OH)_4^-$ solvation shell. Thus, the combined experimental and computational interpretation of the NMR data is consistent with an increase in medium-range $Al(OH)_4^-\cdots Na^+$ interactions (4−6 Å) and, further, the solution ensemble of ion−ion interactions does not have significant populations of contact ion pairs (CIPs). The fact that these medium-range $Al(OH)_4^-\cdots Na^+$ interactions influenced the crystallization process and the product morphology, even in the absence of CIPs, was demonstrated by SEM and XRD analysis of the gibbsite phase, present in high concentrations before and after hydrothermal treatment, and by progressive change in the full width at half-maximum (fwhm) of the O_h resonance, as measured by in situ NMR.

2. EXPERIMENTAL SECTION

2.1. Synthesis of Gibbsite, $Al(OH)_3$. Euhedral hexagonal $Al(OH)_3$ nanoplates with a length of 332 ± 73 nm and a thickness of 29 ± 7 nm were synthesized as described elsewhere, to mitigate the effect of variations in $Al(OH)_3$ particle size and shape on experimental results.[31] Briefly, an aqueous solution of 0.25 M aluminum nitrate nonahydrate ($Al(NO_3)_3{\cdot}9H_2O$, ≥98%, Sigma-Aldrich) was titrated to a pH of ca. 5 with an aqueous solution of 1 M sodium hydroxide (NaOH, ≥98%, Sigma-Aldrich). The resulting gel-like precipitates were stirred for 1 h at room temperature and collected by centrifugation. The collected solid was redispersed in 18 MΩ water and centrifuged three times to remove residual Na^+ and NO_3^-. The washed gel was then dispersed into 18 MΩ water in a Teflon-lined Parr reaction vessel and heated at 80 °C in an oven equipped with a rotating element (ca. 10 rpm). After 3 days, the formed gibbsite nanoplates were collected by centrifugation and washed three times in 18 MΩ water.

2.2. Ex Situ and In Situ ^{27}Al NMR Spectroscopy. Ex situ dissolution studies were performed to constrain the degree of saturation in the experiments. $Al(OH)_3$ dissolution in 3 M NaOH in D_2O was performed in Teflon-lined Parr reaction vessels that were loaded and sealed inside a nitrogen-filled glovebox. Reaction mixtures were stirred for 2 days at room temperature to reach steady state. Following hydrothermal treatment at a range of temperatures from 80 to 100 °C, aliquots of each reaction mixture were then collected, filtered, and analyzed. Ex situ ^{27}Al NMR spectroscopy was carried out on a Varian-Inova 750 MHz NMR narrow-bore spectrometer to obtain detailed information on Al speciation in these solutions. Experiments utilized a 4 mm Teflon insert placed coaxially inside a standard 5 mm solution NMR tube such that the reference aqueous solution (0 ppm) of 1 M aluminum chloride was physically separated from the experimental samples and placed inside the narrow gap between the outer surface of the Teflon tube and inner diameter of the 5 mm tube. This enabled careful and reproducible observation of the Al_{T_d} signal in solutions below and above saturation.

In situ ^{27}Al MAS NMR measurements to simultaneously study the solid and solution phases were carried out on a Varian-Inova 500 MHz NMR spectrometer using a 7.5 mm MAS probe and a novel in situ high-temperature and high-pressure 7.5 mm all-zirconia MAS rotor.[24] The sample spinning rate was 3.8 kHz at a resonance frequency of 130.3 MHz. $Al(OH)_3$ nanoplates were dispersed in 3.00 M NaOH in D_2O to prepare samples containing 0.15, 1.00, and 2.40 M total Al. The samples were subsequently heated to temperatures up to 100 °C at approximately 3 °C min^{-1} and cooled to 25 °C in the NMR instrument. MAS NMR spectra were recorded using a pulse width of 2.5 μs for a $\pi/4$ pulse with a 1 s recycle delay and an acquisition time of 80 ms. Chemical shifts are externally referenced to 1 M $Al(NO_3)_3$ aqueous solution at 0 ppm. Data processing was conducted with a line broadening of 25 Hz.

2.3. Solution-Phase and Solid-Phase Characterization. The presence or absence of Al solution species with a higher degree of polymerization in comparison to the $Al(OH)_4^-$ anion was verified using Raman spectroscopy. Solution-phase Al concentrations were determined using inductively coupled plasma−optical emission spectroscopy (ICP-OES). Analysis of the solid $Al(OH)_3$ phase before and after dissolution/precipitation reactions was conducted using powder X-ray diffraction (XRD) and scanning electron microscopy (SEM), with details provided in the Supporting Information.

2.4. Ab Initio Molecular Dynamics. AIMD simulations were carried out in the canonical ensemble (NVT ensemble) using the Quickstep module of the CP2K software and periodic boundary conditions.[32] Periodic cubic boxes of side 14.35 Å containing one $Al(OH)_4^-$ anion and one Na^+ ion solvated by 90 water molecules were used in the simulations. Three different simulations were carried out where Al to Na distances were fixed at approximately 2.5, 4.0, and 6.2 Å to simulate contact ion pairs (CIP), solvent-separated ion pairs (SSIP), and no pairing-like conditions, respectively. A similar box without the inclusion of Na^+ was used as a reference aluminate solvated system. The temperature was targeted at 300 K using the CSVR[33] (canonical sampling through velocity rescaling) thermostat with a time constant of 20 fs. Valence electrons were treated at the DFT level employing the revPBE functional with dual basis sets DZVP-MOLOPT-SR type with density from a cutoff of 400R. Core electrons on all atoms were represented by Goedecker−Teter−Hutter (GTH) pseudopotentials.[34] The Grimme D3[35] dispersion correction for the revPBE functional was added with a 40 Å cutoff. A time step of 0.5 fs was used to generate the AIMD trajectory. All runs had an equilibration period of 2 ps. $Al(OH)_4^-$ clusters were extracted every 10 fs from the last 3 ps of each simulation for NMR calculations (~300 points). The GIAO method[36−40] as implemented in the Gaussian software package[41] was used to calculate the Al NMR shielding tensor of the resulting clusters at the DFT(B3LYP/6-31G +(d,p)) level of theory.[42]

3. RESULTS

3.1. Activity Coefficients and Mineral Solubility of the Na^+−$Al(OH)_4^-$−OH^- System (PHREEQC). To determine the [Al] required to produce samples that were (i) undersaturated with respect to gibbsite, (ii) at the [Al] solubility limit, and (iii) significantly oversaturated with respect to gibbsite, an updated calculation based on Pitzer coefficients for the gibbsite solubility curve in the system comprising of Na^+, $Al(OH)_4^-$, and OH^- was performed. Details pertaining to this model can be found in the Supporting Information. The solubility curve of gibbsite in solutions of variable sodium hydroxide concentration and temperature are shown in Figure 1 and were used in the design of dissolution and in situ NMR experiments. The experimental conditions of 0.15, 1.0, and 2.4 M gibbsite in 3.0 M NaOH represent, upon cooling to 25 °C, undersaturated (0.15 M) and supersaturated (1.0 and 2.4 M)

DOI: 10.1021/acs.inorgchem.8b00617
Inorg. Chem. 2018, 57, 11864−11873

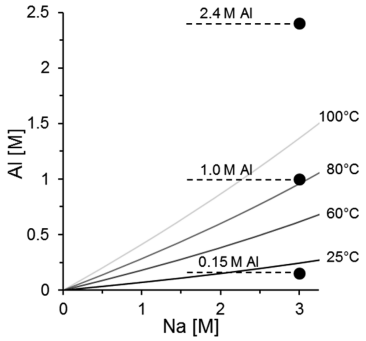

Figure 1. PHREEQC data for the solubility of gibbsite in NaOH at various temperatures.

conditions. The two supersaturated systems are distinguished by the presence of trace (1.0 M) or significant (2.4 M) quantities of undissolved gibbsite at the end of the heating cycle.

3.2. Ex Situ ^{27}Al NMR. The set of experimental conditions chosen based on PHREEQC calculations was initially evaluated using an ex situ approach where NaOH solutions containing appropriate quantities of $Al(OH)_3$ were allowed to react at room temperature for 24 h. ICP-OES analysis conducted on aliquots sampled from these reactions verified the Pitzer ion interaction aqueous model implemented in PHREEQC with the highest experimentally determined concentration being 0.30 ± 0.01 M, which is 0.06 M above the predicted value (see the Supporting Information). It should be noted that the values obtained herein do not correspond to equilibrium conditions, as kinetic measurements necessary to confirm this statement were not performed. The second set of measurements, including ^{27}Al NMR and Raman spectroscopy, were carried out after 24 h (0.15, 0.5, and 1.0 M NaOH) and 3 h (2.4 M NaOH) heating cycles at 80 and 100 °C, respectively, and likewise may not correspond to equilibrium conditions. ICP-OES results show that the 0.15 M (experimental [Al] = 0.13 M) system remains undersaturated, while the 0.5 M (experimental [Al] = 0.42 M), 1.0 M (experimental [Al] = 0.82 M), and 2.4 M (experimental [Al] = 0.77 M) systems become supersaturated upon cooling to room temperature (Figure 1). The seemingly lower solubility of the 2.4 M system, in comparison to the 1.0 M system, is attributed to the shorter heating period.

^{27}Al NMR spectra were collected on a 750 MHz instrument in the presence of physically isolated reference standard ($Al(H_2O)_6^{3+}$, δ = 0 ppm), providing improved resolution and accuracy. Results obtained from the four preheated systems are summarized in Figure 2. A signal in the ca. 80 ppm region of the ^{27}Al spectra is consistent with the presence of tetrahedrally coordinated aluminate ion $Al(OH)_4^-$, with the possibility that the ion pair Na^+-$Al(OH)_4^-$ and the aluminate dimer $Al_2O(OH)_6^{2-}$ are also present in low quantities.[43−45] Analyses of ^{27}Al NMR spectra reveal a near-linear (R^2 = 0.9698) downfield shift of the single observable T_d signal from 80.362 ppm ([Al] = 130 mM) to 80.416 ppm ([Al] = 816 mM) (Tables S1 and S2). This trend is consistent with the downfield shift observed by Sipos et al. as a function of increasing [Al] from 0.005 to 3.0 M, although these subtle effects were not considered in that study, and it was stated that the chemical shift was practically independent of [Al] at [NaOH] < 5 M (i.e., solution compositions of industrial significance).[46] Likewise, a similar trend (R^2 = 0.977) is

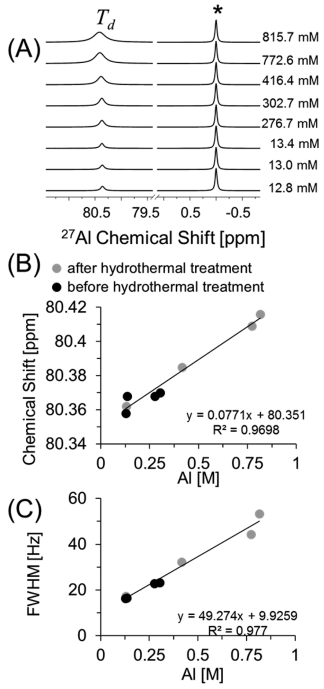

Figure 2. (A) ^{27}Al NMR spectra of the ex situ gibbsite dissolution experiments showing the tetrahedral signal at ca. 80.3 ppm and reference signal at 0 ppm. (B) Changes in chemical shift and (C) full width at half-maximum as a function of aluminum concentration. We note that the linear interpolation uses both the before and after hydrothermal treatment data. The resonance of the physically separated, internal standard is marked with *.

observed for fwhm values that increase from 17.2 Hz ([Al] = 130 mM) to 53.4 Hz ([Al] = 816 mM). Changes in fwhm values have been previously attributed to increased solution viscosity and/or condensation of the monomeric $Al(OH)_4^-$ ions into the oxo-bridged aluminate dimer $Al_2O(OH)_6^{2-}$.[43,44] The conditions implemented in the current study fall outside those associated with substantial dimer formation, and this was confirmed with Raman spectroscopy. Raman spectra of the preheated solutions yielded, in each case, a single peak centered at ca. 600 cm^{-1} indicating the presence of the $Al(OH)_4^-$ ion in a deuterated system (Figure S3).[46] No signals were observed in the region associated with the $Al_2O(OH)_6^{2-}$ dimer (ca. 535 and 705 cm^{-1}).[16,18,43] Furthermore, consistency of the signal position associated with the aluminate ion (600 cm^{-1}) suggests that formation of contact ion pairs, if present, does not contribute significantly to changes observed in this study.[47,48]

3.3. Ab Initio Molecular Dynamics (AIMD). The experimental data lead to the hypothesis that cation−anion interactions occurring at distances longer than contact ion pairs may be responsible for the observed subtle shifts in the ^{27}Al NMR. To test this hypothesis, AIMD simulations were performed to study the relationship between cation−anion distance and the corresponding changes in chemical shift, in comparison to a simulation performed with a solely water solvated $Al(OH)_4^-$ anion. At each fixed $Al(OH)_4^-\cdots Na^+$ distance within the solvated AIMD simulation two different NMR calculations were performed. In the first calculation, the chemical shifts of Al were obtained for the ensemble of 300 $Al(OH)_4^-$ geometries in the presence of the Na^+. In the second calculation, the same ensemble of $Al(OH)_4^-$ geo-

DOI: 10.1021/acs.inorgchem.8b00617
Inorg. Chem. 2018, 57, 11864−11873

metries was considered; however, Na^+ was removed solely from the NMR calculation to establish the effect of the electrostatic effect upon the Al chemical shift. To understand the effect of the Na^+ upon the solvation environment and subsequent geometry of the $Al(OH)_4^-$, as well as the electrostatic effect induced by the presence of Na^+ upon the electronic structure of the $Al(OH)_4^-$, three distinct $Al(OH)_4^-\cdots Na^+$ distances were chosen to compute the Al T_d chemical shift. Here, the "electrostatic effect" encompasses the change in electron density distribution of the Al center caused by the nearby cation. The effect of the Na^+ upon the $Al(OH)_4^-$ geometry versus solely the electrostatic effect upon the chemical shift as a function of the ion−ion distance is represented in Figure 3 (see Table S3 for numerical results).

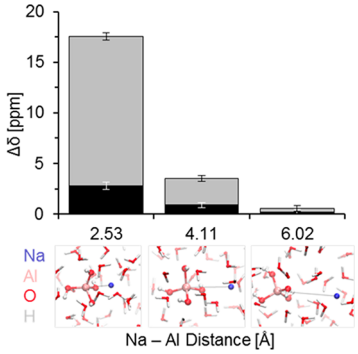

Figure 3. DFT NMR chemical shift calculations breaking down the direct effects of $Al(OH)_4^-$−Na^+ interactions (gray) and the indirect effects of changes in $Al(OH)_4^-$ geometry (black) on the NMR shielding tensor. $Al(OH_4)^-$ solvated simulation boxes with Na^+ included at Al−Na distances of (A) 2.5 Å, (B) 4.1 Å, and (C) 6.0 Å.

Both the geometric and electrostatic effects influence the ^{27}Al NMR chemical shift. However, the electrostatic contribution predominates below an ion−ion distance of 6 Å. Small shifts are observed from 6 Å down to the formation of the solvent-separated ion pair at ∼4 Å; however, upon formation of the SSIP, the change in the chemical shift becomes more significant as the geometric contribution also increases, a feature that is enhanced upon contact ion pair formation.[23]

Although the electrostatic effect upon the ^{27}Al NMR begins to perturb the chemical shift at medium distances, the geometric perturbation cannot be discounted as SSIP and CIPs are formed. In an effort to understand the influence of the Na^+ ion on the solvation structure (and in turn the aluminate response to the changes in solvation), we considered the fluctuations about a fixed frame constructed from the aluminate tetrahedral ion, $Al(OH)_4^-$. The Al was placed at the origin of the coordinate system, with the shortest Al−O bond along the x axis and nearest O to the Al in the x−y plane. The atomic position of the Al (which is fixed in the coordinate system), was then superimposed with the positions of the hydroxyl ligands, the Na^+, and solvating H_2O O atoms over an ensemble of 600 snapshots from AIMD (Figure 4). In comparison to the reference system of aluminate in pure water, it is evident that the presence of the Na^+ at 2.5 Å from the Al center tends to localize the position of the H on the hydroxyl group. This is further demonstrated in Figure S10, where the distribution of the H−O−Al−O dihedral angle is plotted. Here the peaks in the structure quantify this localization. Note too in Figure 4 how the spherical access of

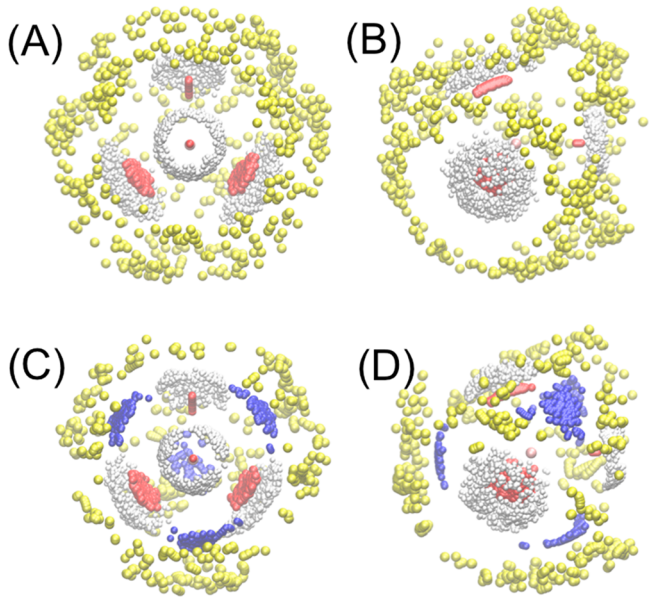

Figure 4. Presence of Na^+ ions resulting in modification of internal structure (blue Na^+, white H, red internal O on OH) as well as solvation structure (yellow O on H_2O). (A) and (B) correspond to the ensemble of atomic positions of aluminate in pure water, while (C) and (D) correspond to the ensemble of atomic positions at an Al−Na^+ distance of 2.5 Å (the contact ion pair). (A) and (C) present views along the fixed Al−O bond, while (B) and (D) are rotated 90° with respect to that frame of reference.

the nearest water is significantly restricted in the contact ion pair (Al−Na distance of 2.5 Å) in comparison to the pure water reference system. These features in the internal structure as well as the surrounding solvent structure are expected to influence the NMR chemical shift and lead to changes in the geometric contribution to the Al chemical shift in Figure 3. Note that these calculations do not represent a quantitative comparison to experiment, as the proper weighting of the ensemble configurations is not taken into account. Instead this study qualitatively shows that medium distance range ion−ion interactions are likely the fundamental source of the small chemical shifts to Al observed under the experimental conditions and further that high populations of contact ion pairs must not be present in the experimental solution ensemble. In solutions with higher [Al], there should be both an increase in the frequency of interaction between $Al(OH)_4^-$ anions and Na^+ cations and a concomitant overall decrease in ion−ion distances. For the first time, AIMD simulations have been used to predict that this would result in a decrease in the shielding tensor and a downfield chemical shift, which is consistent with the results in Figure 2B and in earlier work by Sipos et al.[23] Note that this is the opposite trend to the effect of increasing [NaOH], which leads to an upfield chemical shift due to the formation of contact ion pairs between the Na^+ and the $Al(OH)_4^-$ or the presence of dimeric aluminate species.[46] These changes in speciation result in increased $Al(OH)_3$ solubility,[49] whereas increasing [Al] ultimately leads to $Al(OH)_3$ precipitation. The subtle angular and distance perturbations in the aluminate structure observed and simulated here (see Figure S10) may represent the early stages of this precipitation process. In a complementary Al K-edge X-ray absorption near edge structure (XANES) study of 0.5 M $Al(OH)_3$ in a 2.7 M hydroxide solution containing

DOI: 10.1021/acs.inorgchem.8b00617
Inorg. Chem. 2018, 57, 11864−11873

either 2.7 M sodium or 8.5 M sodium (augmented with sodium nitrate), a shift in the pre-edge shoulder correlated to sodium concentration was observed, and the physical origin of that shift was also attributed to these longer-range ion interactions using energy-specific time-dependent density functional theory of subensembles obtained from ab initio molecular dynamics.[50]

3.5. In Situ ^{27}Al NMR. While ex situ analysis of the solution-phase Al provided much-needed information on changes to the ion−ion interactions within the ensemble solution configurations as a function of experimental [Al], to obtain a complete picture of the dissolution/precipitation reaction, in situ ^{27}Al MAS NMR is needed to allow Al^{3+} in both the solid and solution phases to be studied simultaneously. A sample containing 1.0 M gibbsite and 3.0 M NaOH was prepared to investigate conditions exceeding the solubility limit of Al at NaOH concentrations commonly found in high-level nuclear waste awaiting processing for long-term disposal at the Hanford Site. The results are summarized in Figure 5.

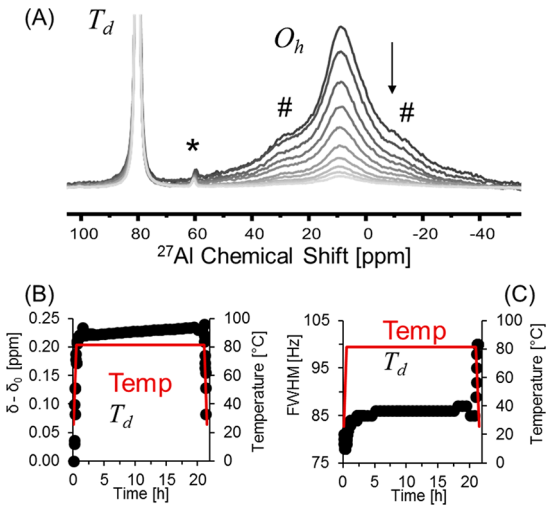

Figure 5. 1.0 M gibbsite dissolved in 3 M NaOH. (A) In situ NMR spectra as the temperature increases to 80 °C with emphasis on the O_h region. (B) Changes in chemical shift observed in the T_d resonance. (C) fwhm of the T_d resonance. In the NMR spectra, spin lines of the O_h resonance are denoted with # and spin lines of the T_d resonance are denoted with *.

The T_d resonance, corresponding to solution species ($Al(OH)_4^-$), and the O_h resonance, corresponding to the solid gibbsite ($Al(OH)_3$), are simultaneously resolved with the in situ MAS NMR technique (Figure 5a). We observe a steady increase in the proportion of the T_d resonance with respect to O_h as the temperature changes from ∼25 °C to 80 °C, which is consistent with gradual dissolution of gibbsite and formation of a tetrahedral aluminate ion. This change corresponds with an increase in T_d fwhm from 81 to 84 Hz during the heating ramp. One would expect the fwhm to decrease as the temperature increases due to a decrease in solution viscosity. However, the increase in temperature also corresponds with an increase in the concentration of T_d species, as stated above, and an increase in the thermal vibrations of the Al−OH bonds. We propose that the superposition of these three phenomena (i.e., increased [Al], increased Al−OH thermal vibrations, and decreased viscosity) results in the observed fwhm trend during the temperature ramp to 80 °C. We note that direct comparison of the absolute fwhm values between the ex situ and the in situ experiments is not possible due to differences in field strengths. However, the overall trend is consistent; as the effective [Al] in solution increases, the fwhm increases. The subsequent cooling step (T_{final} ≈ 25 °C) coincides with a further increase in fwhm to 100 Hz, consistent with increased solution viscosity.

The observed chemical shift of T_d species increases by 0.082 ppm between the start and the end of the experiment (∼25 °C), an increase which is consistent with increased [Al] in solution. This result is in good agreement with trends observed in the ex situ 750 MHz experiment and is consistent with computationally predicted formation of medium range solvent separated ion pairs. We also note chemical shift drifts of ca. 0.009 ppm at 80 °C over the course of many hours. This is likely due to drift in the magnetic field, which would be ameliorated by development of an in situ rotor incorporating a coaxial insert. This limitation prohibits detailed analysis of subtle changes in the T_d chemical shift during in situ experiments, but by estimation of the drift by the observed change at 80 °C, the overall change in chemical shift is ca. 0.073 ppm. This result is consistent with the change observed in the ex situ experiments (0.054 ppm). The supersaturated [Al] = 1.0 M system was confirmed to be stable at room temperature in the NMR instrument for 3.5 h without sign of nucleation, as indicated by a lack of signals corresponding to O_h species (Figure S6). Similar overall trends were observed for in situ experiments conducted on the undersaturated system (0.15 M gibbsite, 3.0 M NaOH, see the Supporting Information).

During the dissolution of the solid-state O_h Al in $Al(OH)_3$ to form solution-phase T_d Al as $Al(OH)_4^-$, the potential for an intermediary pentacoordinated Al complex must be considered. Recent MD simulations suggest that $Al(OH)_3$ dissolution occurs through short-lived pentacoordinated Al ions in solution and through dangling ledge adatoms on $Al(OH)_3$.[51] However, a quantitative NMR study of $Al(OH)_3$ crystallization demonstrated that, although it was possible to detect low-coordinated Al species at concentrations as low as 0.1%, these sites were solvated by water under hydrated conditions and exhibited O_h coordination. In this work, broad spinning sidebands (Figure 5A, sidebands indicated with #) originating from the solid-phase O_h Al occur in the typical range of pentacoordinated Al species (41−31 ppm),[52] limiting the potential for detection of Al in this coordination environment. Thus, the presence of a small fraction of pentacoordinated Al on the surface of gibbsite cannot be ruled out during the dissolution process in this system, but quantification of this coordination environment is beyond the detection limit of the in situ NMR experiments.

Samples far exceeding the solubility limit of gibbsite in 3.0 M NaOH were investigated by heating a sample containing an initial gibbsite concentration of 2.4 M from ∼25 to 100 °C, briefly establishing hydrothermal conditions. As shown in Figure 6, and previously predicted using the PHREEQC model, the octahedral phase does not fully dissolve during the course of the experiment, providing an opportunity to evaluate the effect of the brief hydrothermal treatment on the undissolved gibbsite and the associated solution species. The overall trends observed in the solution-phase T_d signal are comparable to those of the 1.0 M [Al] experiment and are described in full detail in Figure S7 in the Supporting Information. We summarize important differences. Mainly,

DOI: 10.1021/acs.inorgchem.8b00617
Inorg. Chem. 2018, 57, 11864−11873

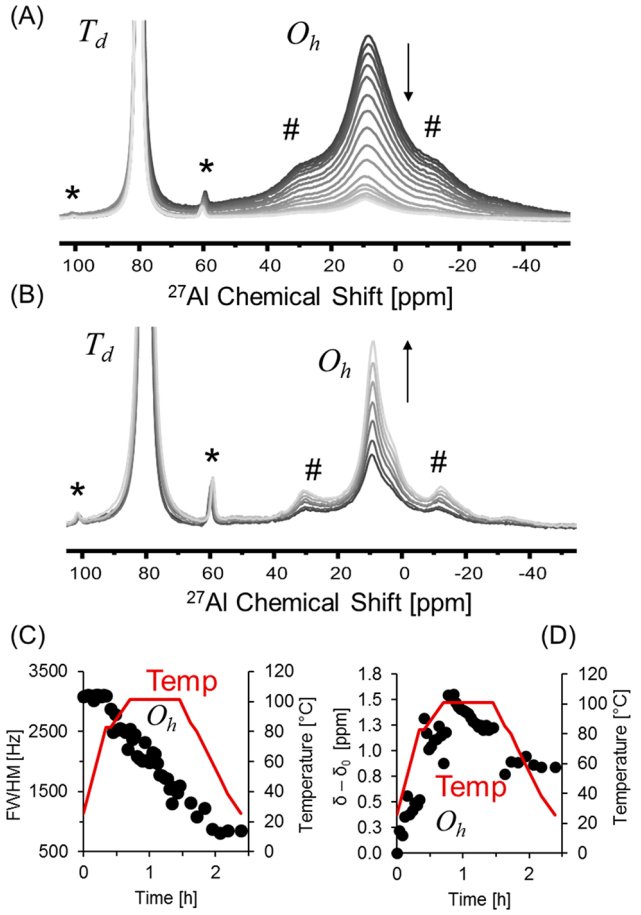

Figure 6. 2.4 M gibbsite dissolved in 3 M NaOH. (A) In situ NMR spectra as the temperature was increased to 100 °C with emphasis on the O_h region. (B) In situ NMR spectra as the temperature was decreased to 25 °C with emphasis on the O_h region. (C) fwhm of the O_h resonance. (D) Changes in chemical shift observed in the O_h resonance. In the NMR spectra, spin lines of the O_h resonance are denoted with # and spin lines of the T_d resonance are denoted with *.

the value of fwhm decreased from 92 to 81 Hz during the temperature ramp to 100 °C, which was not observed in the 1.0 M system, but increased to 116 Hz upon returning the system to ~25 °C, showing an overall increase of 24 Hz. The chemical shift is observed to drift downfield at 100 °C (ca. 0.0577 ppm). The cause of this drift is likely due to (i) drift of the magnetic field and (ii) changes in the relative T_d to O_h ratio consistent with continuous dissolution of $Al(OH)_3$ through the course of this brief hydrothermal treatment. Overall, the changes observed for the T_d resonance are consistent with these observed in the previous in situ and ex situ experiments: that is, formation of medium range solvent separated ion pairs. It is possible that the inverse trend observed for the fwhm during the initial heating cycle (~25 to 100 °C) is caused by interactions of $Al(OH)_4^-$ with excess solid phase.

The O_h resonance, in contrast, showed significant changes as a result of the hydrothermal treatment. The intensity of the O_h resonance fluctuated as a function of the reaction coordinate, reaching a minimum value consequent to completion of the heating step and showing slow, but progressive, growth thereafter. This result can be interpreted as initial dissolution of the $Al(OH)_3$ phase resulting under supersaturated conditions and subsequent minor precipitation events. Changes in the relative abundance of the O_h resonance coincide with a drastic decrease in the fwhm from 3100 Hz at the start of the reaction to 750 Hz at the end point and a 0.9 ppm downfield shift of the signal. To evaluate the cause for this significant change in O_h fwhm, complementary SEM and XRD measurements were collected to further characterize the changes in the residual solid phase.

3.6. Solid-State Characterization. XRD and SEM characterization of residual $Al(OH)_3$ (2.4 M) from hydrothermal treatment for 1 h at 100 °C in 3 M NaOH were used to investigate changes in crystallinity and morphology (Figure 7). These conditions were selected to maximize the [Al] in solution but to limit transformation of the solid phase from gibbsite to boehmite. Previous work[25] and recent experimental results have shown that, at temperatures ≤100 °C, and at short reactions times governed by kinetics rather than thermodynamics, gibbsite (in the presence of gibbsite as crystallization templates) remains the dominant solid-phase product. XRD analysis after the short exposure to 100 °C in this study confirmed the presence of only gibbsite (Figure S8). Evaluation of fwhm values from obtained PXRD patterns using DIFFRAC.SUITE TOPAS suggested changes in crystal domain size from 33.3 ± 2.7 nm before to 50.4 ± 1.4 nm after the hydrothermal treatment. Morphology analysis by SEM suggested the growth of gibbsite nanoparticles in length and thickness during the hydrothermal treatment, consistent with simultaneous dissolution and reprecipitation, with an approximate 77% increase in the thickness/length aspect ratio. These observations confirm that supersaturation, with concurrent changes in speciation, affect the crystallization mechanism and thus the crystal morphology.[53,54] The change in thickness/length aspect ratio suggests that preferential growth of the prismatic, i.e. (101) and (100), faces occurs.

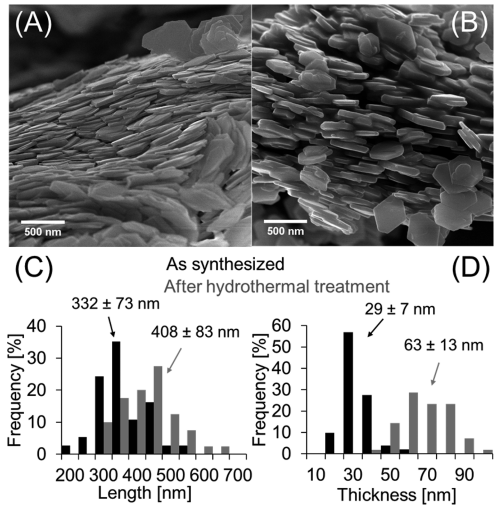

Figure 7. (A) SEM of gibbsite as synthesized. (B) SEM of gibbsite after hydrothermal treatment. (C) Histogram of the length of the gibbsite nanoplates as synthesized and after hydrothermal treatment. (D) Histogram of the thickness of the gibbsite nanoplates as synthesized and after hydrothermal treatment.

4. CONCLUSIONS

In situ NMR spectroscopy, solid-state characterization techniques, and high-level molecular dynamics simulations combined to explore interactions between solution-phase $Al(OH)_4^-$ anions and Na^+ cations in the presence and absence

DOI: 10.1021/acs.inorgchem.8b00617
Inorg. Chem. 2018, 57, 11864−11873

of solid-phase $Al(OH)_3$ under 3 M NaOH conditions relevant to high-level radioactive tank waste processing have provided key new insights into conditions at the molecular scale incipient and concurrent with gibbsite crystallization. Precise ex situ NMR experiments utilizing coaxial inserts allowed detection of a minor downfield T_d chemical shift. This is correlated to predicted subtle changes in the electron density distribution about the $Al(OH)_4^-$ anion in solution due to medium range ion−ion interactions at hydroxide concentrations where such subtle shifts have not previously been observed. Novel in situ NMR experiments highlighted the overall stability of the solvation structure for T_d in the $Al(OH)_4^-$ anion, as the chemical shift varied very little as a function of temperature and [Al] in 3.0 M NaOH solutions. [Al] in solution remained above saturation up to 1.0 M, with limited precipitation of an octahedral $Al(OH)_3$ phase upon cooling from 80 or 100 °C, over the observed 3.5 h time scale for the 1 M [Al] experiment, despite a thermodynamically derived solubility limit of 0.245 M at room temperature. Ab initio molecular dynamics simulations complemented with DFT-based chemical shift calculations further highlight the overall stability of the solvation structure for T_d Al in the $Al(OH)_4^-$ oxyanion, indicating that measurable perturbations should begin when the $Al(OH)_4^-\cdots Na^+$ distance is less than 6 Å, coinciding with appreciable changes to the electrostatic interaction and reorganization of the $Al(OH)_4^-$ solvation shell. The findings thus suggest that, during gibbsite crystallization under these conditions, nominally expected contact ion pairs are insignificant and instead medium-range (4−6 Å) solvent-separated $Al(OH)_4^-\cdots Na^+$ pairs predominate. Progressive changes in the fwhm of the O_h resonance of residual gibbsite correlated with increases in particle size and crystallinity observed with XRD and SEM. These integrated findings suggest that medium-range solvent-separated $Al(OH)_4^-\cdots Na^+$ interactions dominate $Al(OH)_4^-$ speciation in solution incipient to and concurrent with gibbsite crystallization and that sluggish gibbsite precipitation may arise from the activation energy associated with disrupting this robust interaction.

■ ASSOCIATED CONTENT

Supporting Information

The Supporting Information is available free of charge on the ACS Publications website at DOI: 10.1021/acs.inorgchem.8b00617.

Experimental methodology and PHREEQC and other experimental results (PDF)

■ AUTHOR INFORMATION

Corresponding Author

*C.I.P.: e-mail, carolyn.pearce@pnnl.gov; tel, +1 (509) 372−4875.

ORCID

Xin Zhang: 0000-0003-2000-858X
Nicholas R. Jaegers: 0000-0002-9930-7672
Jianzhi Hu: 0000-0001-8879-747X
Hsiu-Wen Wang: 0000-0002-2802-4122
Andrew G. Stack: 0000-0003-4355-3679
Aurora E. Clark: 0000-0001-9381-721X
Kevin M. Rosso: 0000-0002-8474-7720
Carolyn I. Pearce: 0000-0003-3098-1615

Author Contributions

#T.R.G. and M.D. contributed equally.

Notes

The authors declare no competing financial interest.

■ ACKNOWLEDGMENTS

This work was supported by IDREAM (Interfacial Dynamics in Radioactive Environments and Materials), an Energy Frontier Research Center funded by the U.S. Department of Energy (DOE), Office of Science, Basic Energy Sciences (BES). Materials characterization and NMR measurements were performed using the Environmental Molecular Science Laboratory (EMSL), a national scientific user facility sponsored by the DOE Office of Biological and Environmental Research and located at Pacific Northwest National Laboratory (PNNL). This research used resources of the Oak Ridge Leadership Computing Facility located in the Oak Ridge National Laboratory, which is supported by the Office of Science within the Department of Energy under Contract No. DE-AC05-00OR22725. The authors thank Chuan Wan and Mary Hu for their assistance with the in situ MAS NMR experiments. T.R.G. is grateful for support from the PNNL-WSU DGRP. PNNL is a multiprogram national laboratory operated for DOE by Battelle Memorial Institute under Contract No. DE-AC06-76RLO-1830.

■ REFERENCES

(1) Reynolds, J. G.; McCoskey, J. K.; Herting, D. L. Gibbsite Solubility in Hanford Nuclear Waste Approached from above and below Saturation. *Ind. Eng. Chem. Res.* **2016**, *55*, 5465−5473.

(2) Pereira, J. A. M.; Schwaab, M.; Dell'Oro, E.; Pinto, J. C.; Monteiro, J. L. F.; Henriques, C. A. The Kinetics of Gibbsite Dissolution in NaOH. *Hydrometallurgy* **2009**, *96*, 6−13.

(3) Yang, H.; Pan, X.; Yu, H.; Tu, G.; Sun, J. Dissolution Kinetics and Mechanism of Gibbsitic Bauxite and Pure Gibbsite in Sodium Hydroxide Solution under Atmospheric Pressure. *Trans. Nonferrous Met. Soc. China* **2015**, *25*, 4151−4159.

(4) Grénman, H.; Salmi, T.; Murzin, D. Y.; Addai-Mensah, J. The Dissolution Kinetics of Gibbsite in Sodium Hydroxide at Ambient Pressure. *Ind. Eng. Chem. Res.* **2010**, *49*, 2600−2607.

(5) Bao, L.; Zhang, T.; Liu, Y.; Dou, Z.; Lü, G.; Wang, X.; Ma, J.; Jiang, X. The Most Probable Mechanism Function and Kinetic Parameters of Gibbsite Dissolution in NaOH. *Chin. J. Chem. Eng.* **2010**, *18*, 630−634.

(6) Li, X.; Yan, L.; Zhou, Q.; Liu, G.; Peng, Z. Thermodynamic Model for Equilibrium Solubility of Gibbsite in Concentrated NaOH Solutions. *Trans. Nonferrous Met. Soc. China* **2012**, *22*, 447−455.

(7) Bao, L.; Nguyen, A. V. Developing a Physically Consistent Model for Gibbsite Leaching Kinetics. *Hydrometallurgy* **2010**, *104*, 86−98.

(8) Bourrié, G.; Grimaldi, C.; Régeard, A. Monomeric versus Mixed Monomeric-Polymeric Models for Aqueous Aluminium Species: Constraints from Low-Temperature Natural Waters in Equilibrium with Gibbsite under Temperate and Tropical Climate. *Chem. Geol.* **1989**, *76*, 403−417.

(9) Bloom, P. R.; Erich, M. S. Effect of Solution Composition on the Rate and Mechanism of Gibbsite Dissolution in Acid Solutions. *Soil Sci. Soc. Am. J.* **1987**, *51*, 1131−1136.

(10) Shen, Z.; Kerisit, S.; Stack, A.; Rosso, K. Free Energy Landscape of the Dissolution of Gibbsite at High pH. *J. Phys. Chem. Lett.* **2018**, *9*, 1809.

(11) Sipos, P.; Schibeci, M.; Peintler, G.; May, P. M.; Hefter, G. Chemical Speciation in Concentrated Alkaline Aluminate Solutions in Sodium, Potassium and Caesium Media. Interpretation of the Unusual Variations of the Observed Hydroxide Activity. *Dalt. Trans.* **2006**, *15*, 1858.

DOI: 10.1021/acs.inorgchem.8b00617
Inorg. Chem. 2018, 57, 11864−11873

(12) Zhang, J.; Klasky, M.; Letellier, B. C. The Aluminum Chemistry and Corrosion in Alkaline Solutions. *J. Nucl. Mater.* **2009**, *384*, 175−189.
(13) Li, X.; Wang, D.; Zhou, Q.; Liu, G.; Peng, Z. Concentration Variation of Aluminate Ions during the Seeded Precipitation Process of Gibbsite from Sodium Aluminate Solution. *Hydrometallurgy* **2011**, *106*, 93−98.
(14) Johnston, C. T.; Agnew, S. F.; Schoonover, J. R.; Kenney, J. W.; Page, B.; Osborn, J.; Corbin, R. Raman Study of Aluminum Speciation in Simulated Alkaline Nuclear Waste. *Environ. Sci. Technol.* **2002**, *36*, 2451−2458.
(15) Schoonover, J. R.; Zhang, S. L.; Johnston, C. T. Raman Spectroscopy and Multivariate Curve Resolution of Concentrated Al_2O_3 − Na_2O-H_2O Solutions. *J. Raman Spectrosc.* **2003**, *34*, 404−412.
(16) Sipos, P.; Hefter, G.; May, P. M. ^{27}Al NMR and Raman Spectroscopic Studies of Alkaline Aluminate Solutions with Extremely High Caustic Content − Does the Octahedral Species $Al(OH)_6^{3-}$ Exist in Solution? *Talanta* **2006**, *70*, 761−765.
(17) Li, J.; Prestidge, C. A.; Addai-Mensah, J. The Influence of Alkali Metal Ions on Homogeneous Nucleation of Al(OH)33 crystals from Supersaturated Caustic Aluminate Solutions. *J. Colloid Interface Sci.* **2000**, *224*, 317−324.
(18) Sipos, P.; May, P. M.; Hefter, G. Quantitative Determination of an Aluminate Dimer in Concentrated Alkaline Aluminate Solutions by Raman Spectroscopy. *Dalt. Trans.* **2006**, *2*, 368−375.
(19) Pouvreau, P.; Dembowski, D.; Clark, S. B.; Reynolds, J. G.; Rosso, K. M.; Schenter, G. K.; Pearce, C. I.; Clark, A. E. Ab Initio Molecular Dynamics Reveal Spectroscopic Siblings and Ion Pairing as New Challenges for Elucidating Prenucleation Aluminum Speciation. *J. Phys. Chem. B* **2018**, *122*, 7394.
(20) Watling, H. R.; Fleming, S. D.; van Bronswijk, W.; Rohl, A. L. Ionic Structure in Caustic Aluminate Solutions and the Precipitation of Gibbsite. *J. Chem. Soc., Dalton Trans.* **1998**, *23*, 3911−3918.
(21) Buchner, R.; Sipos, P.; Hefter, G.; May, P. M. Dielectric Relaxation of Concentrated Alkaline Aluminate Solutions. *J. Phys. Chem. A* **2002**, *106*, 6527−6532.
(22) Addai-Mensah, J.; Li, J.; Prestidge, C. A. The Structure and Interactions of Species in Supersaturated Caustic Aluminate Solutions. *Dev. Chem. Eng. Miner. Process.* **2002**, *10*, 553−566.
(23) Sipos, P. The Structure of Al(III) in Strongly Alkaline Aluminate Solutions — A Review. *J. Mol. Liq.* **2009**, *146*, 1−14.
(24) Hu, J. Z.; Hu, M. Y.; Zhao, Z.; Xu, S.; Vjunov, A.; Shi, H.; Camaioni, D. M.; Peden, C. H. F.; Lercher, J. A. Sealed Rotors for in Situ High Temperature High Pressure MAS NMR. *Chem. Commun.* **2015**, *51*, 13458−13461.
(25) Wefers, K.; Misra, C. Oxides and Hydroxides of Aluminum. *Alcoa Technol. Pap.* **1987**, *19*, 1−100.
(26) Gale, J. D.; Rohl, A. L.; Watling, H. R.; Parkinson, G. M. Theoretical Investigation of the Nature of Aluminum-Containing Species Present in Alkaline Solution. *J. Phys. Chem. B* **1998**, *102*, 10372−10382.
(27) Watling, H. R.; Fleming, S. D.; Van Bronswijk, W.; Rohl, A. L.; Parker, A. J. Ionic Structure in Caustic Aluminate Solutions and the Precipitation of Gibbsite. *J. Chem. Soc., Dalton Trans.* **1998**, 3911−3918.
(28) Truflandier, L. a.; Autschbach, J. Probing the Solvent Shell with ^{195}Pt Chemical Shifts: Density Functional Theory Molecular Dynamics Study of Pt II and Pt IV Anionic Complexes in Aqueous Solution. *J. Am. Chem. Soc.* **2010**, *132*, 3472−3483.
(29) Truflandier, L. A.; Sutter, K.; Autschbach, J. Solvent Effects and Dynamic Averaging of ^{195}Pt NMR Shielding in Cisplatin Derivatives. *Inorg. Chem.* **2011**, *50*, 1723−1732.
(30) Sterzel, M.; Autschbach, J. Toward an Accurate Determination of ^{195}Pt Chemical Shifts by Density Functional Computations: The Importance of Unspecific Solvent Effects and the Dependence of Pt Magnetic Shielding Constants on Structural Parameters. *Inorg. Chem.* **2006**, *45*, 3316−3324.
(31) Zhang, X.; Zhang, X.; Graham, T. R.; Pearce, C. I.; Mehdi, B. L.; N'Diaye, A. T.; Kerisit, S.; Browning, N. D.; Clark, S. B.; Rosso, K. M. Fast Synthesis of Gibbsite Nanoplates and Process Optimization Using Box-Behnken Experimental Design. *Cryst. Growth Des.* **2017**, *17*, 6801−6808.
(32) VandeVondele, J.; Krack, M.; Mohamed, F.; Parrinello, M.; Chassaing, T.; Hutter, J. QUICKSTEP: Fast and Accurate Density Functional Calculations Using a Mixed Gaussian and Plane Waves Approach. *Comput. Phys. Commun.* **2005**, *167*, 103−128.
(33) Bussi, G.; Donadio, D.; Parrinello, M. Canonical Sampling through Velocity Rescaling. *J. Chem. Phys.* **2007**, *126*, 014101.
(34) Goedecker, S.; Teter, M.; Hutter, J. Separable Dual-Space Gaussian Pseudopotentials. *Phys. Rev. B: Condens. Matter Mater. Phys.* **1996**, *54*, 1703−1710.
(35) Grimme, S.; Antony, J.; Ehrlich, S.; Krieg, H. A Consistent and Accurate Ab Initio Parametrization of Density Functional Dispersion Correction (DFT-D) for the 94 Elements H-Pu. *J. Chem. Phys.* **2010**, *132*, 154104.
(36) London, F. Théorie Quantique Des Courants Interatomiques Dans Les Combinaisons Aromatiques. *J. Phys. Radium* **1937**, *8*, 397−409.
(37) McWeeny, R. Perturbation Theory for the Fock-Dirac Density Matrix. *Phys. Rev.* **1962**, *126*, 1028−1034.
(38) Ditchfield, R. Self-Consistent Perturbation Theory of Diamagnetism. *Mol. Phys.* **1974**, *27*, 789−807.
(39) Wolinski, K.; Hinton, J. F.; Pulay, P. Efficient Implementation of the Gauge-Independent Atomic Orbital Method for NMR Chemical Shift Calculations. *J. Am. Chem. Soc.* **1990**, *112*, 8251−8260.
(40) Cheeseman, J. R.; Trucks, G. W.; Keith, T. A.; Frisch, M. J. A Comparison of Models for Calculating Nuclear Magnetic Resonance Shielding Tensors. *J. Chem. Phys.* **1996**, *104*, 5497−5509.
(41) Frisch, M. J.; Trucks, G. W.; Schlegel, H. B.; Scuseria, G. E.; Robb, M. A.; Cheeseman, J. R.; Scalmani, G.; Barone, V.; Mennucci, B.; Petersson, G. A., et al.. *Gaussian 09*; Gaussian Inc., Wallingford, CT, 2009.
(42) Becke, A. D. Density-Functional Thermochemistry. III. The Role of Exact Exchange. *J. Chem. Phys.* **1993**, *98* (7), 5648.
(43) Moolenaar, R. J.; Evans, J. C.; McKeever, L. D. Structure of the Aluminate Ion in Solutions at High pH. *J. Phys. Chem.* **1970**, *74*, 3629−3636.
(44) Akitt, J. W.; Gessner, W. Aluminium-27 Nuclear Magnetic Resonance Investigations of Highly Alkaline Aluminate Solutions. *J. Chem. Soc., Dalton Trans.* **1984**, 147.
(45) Sipos, P. The Structure of Al(III) in Strongly Alkaline Aluminate Solutions - A Review. *J. Mol. Liq.* **2009**, *146*, 1−14.
(46) Watling, H. Spectroscopy of Concentrated Sodium Aluminate Solutions. *Appl. Spectrosc.* **1998**, *52* (2), 250−258.
(47) Hester, R. E.; Plane, R. A. A Raman Spectrophotometric Comparison of Interionic Association in Aqueous Solutions of Metal Nitrates, Sulfates, and Perchlorates. *Inorg. Chem.* **1964**, *3* (5), 769−770.
(48) Tossell, J. A. Theoretical Studies on Aluminate and Sodium Aluminate Species in Models for Aqueous Solution: $Al(OH)_3$, $Al(OH)_4^-$, and $NaAl(OH)_4$. *Am. Mineral.* **1999**, *84*, 1641−1649.
(49) Reynolds, J. G.; Reynolds, D. A. *A Modern Interpretation of the Barney Diagram for Aluminum Solubility in Tank Waste*; WM2010 Conference, March 7−11, 2010, Phoenix, AZ.
(50) Wildman, A.; Martinez-Baez, E.; Fulton, J.; Schenter, G.; Pearce, C.; Clark, A. E.; Li, X. Anticorrelated Contributions to Pre-Edge Features of Aluminate Near-Edge X-Ray Absorption Spectroscopy in Concentrated Electrolytes. *J. Phys. Chem. Lett.* **2018**, *9*, 2444−2449.
(51) Shen, Z.; Kerisit, S. N.; Stack, A. G.; Rosso, K. M. Free-Energy Landscape of the Dissolution of Gibbsite at High pH. *J. Phys. Chem. Lett.* **2018**, *9*, 1809−1814.
(52) Hu, J. Z.; Zhang, X.; Jaegers, N. R.; Wan, C.; Graham, T. R.; Hu, M.; Pearce, C. I.; Felmy, A. R.; Clark, S. B.; Rosso, K. M. Transitions in Al Coordination during Gibbsite Crystallization Using

DOI: 10.1021/acs.inorgchem.8b00617
Inorg. Chem. 2018, 57, 11864−11873

High-Field ^{27}Al and ^{23}Na MAS NMR Spectroscopy. *J. Phys. Chem. C* **2017**, *121*, 27555−27562.
(53) Childs, C. W.; Hayashi, S.; Newman, R. H. Five-Coordinate Aluminum in Allophane. *Clays Clay Miner.* **1999**, *47*, 64−69.
(54) Loh, J. S. C.; Watling, H. R.; Parkinson, G. M. The Effect of Isotopic Substitution of Deuterium for Hydrogen on the Morphology of Products Precipitated from Synthetic Bayer Solutions. *J. Cryst. Growth* **2002**, *237*−*239*, 2178−2182.

NOTE ADDED AFTER ASAP PUBLICATION

This paper was published July 23, 2018. Reference 19 has been added. The revised version was re-posted July 27, 2018.

DOI: 10.1021/acs.inorgchem.8b00617
Inorg. Chem. 2018, 57, 11864−11873